Computational Final Project

Statistical Physics 2

https://github.com/mschuylermoss/705Project

Schuyler Moss

April 17, 2023

PHYS 705

Problem 1: Two-Dimensional Ferromagnetic Ising Model

In the first part of this project, we are asked to study the two-dimensional Ising model, which is defined by the following Hamiltonian,

$$\hat{H} = -\sum_{\langle ij \rangle} \sigma_i \sigma_j. \tag{1}$$

Here, σ_i, σ_j are Ising spins that take Ising degrees of freedom (± 1), and the sum is taken over nearest neighbors, $\langle ij \rangle$. I consider finite-size square lattices with periodic boundary conditions up to a lattice length of $L = 24$.

This model hosts two distinct phases: the ferromagnetic phase, where all of the spins are aligned in the same direction (ordered), and the paramagnetic phase, where the spins are not aligned in the same direction (disordered). The transition between these phases occurs at a finite temperature, $T_c = 1/\log(1 + \sqrt{2})$, which is given by the Onsager solution [1] and below which the Z_2 symmetry of the system is broken. The order parameter of this transition, which describes the quantity that breaks the symmetry of the system, is the magnetization which is given by the sum over all spins,

$$M = \sum_i \sigma_i. \tag{2}$$

Note that there are two possible "instances" of the ordered phase: one where all of the spins are up and one where all of the spins are down. Importantly, these two cases will have different magnetizations ($M = +N$ and $-N$, respectively). This will be relevant in later analyses.

In order to extract universal behavior of this phase transition from our finite-size Monte Carlo simulations, I track observables that can capture this behavior. Rather than keeping individual estimates of these observables at each Monte Carlo step, we track the average value across these Monte Carlo steps,

$$\langle O \rangle = \frac{1}{m} \sum_i^m O_i. \tag{3}$$

This provides an estimate for a thermodynamic average of that observable. Here, I track $\langle E \rangle$, $\langle E^2 \rangle$, $\langle |M| \rangle$, $\langle M^2 \rangle$, which allows me to calculate the specific heat, C_v, and the magnetic susceptibility, χ_T. The derivations for the calculations of these quantities from the thermodynamic averages are provided below.

Part A

The figures below display E/N (raw values) and $\langle E \rangle / N$ (full average) as a function of Monte Carlo step for $\beta = 1, 3$.

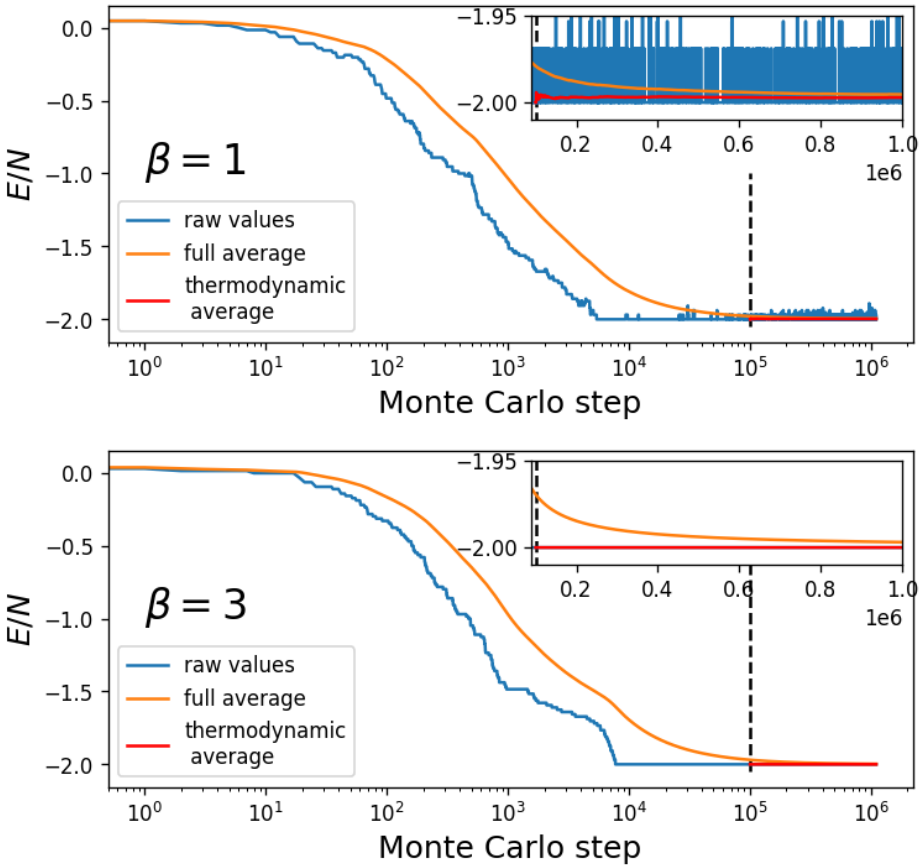

Figure 1: Energy per spin tracked during Monte Carlo simulations.

As seen in the raw values, initially there is a lot of fluctuation in the energy as the Markov chain converges. The full average, which is a running average taken over *all* of the Monte Carlo steps, reflects this, even after many Monte Carlo steps. This period of initial fluctuation/convergence is referred to as the "warm-up" period, and the values of observables calculated during this period are typically ignored when estimating thermodynamic averages. For this reason, I also show the thermodynamic averages in the figures above. These are calculated by taking the running average of the observable of interest, in this case, the energy, but only over the Monte Carlo steps *after* the warm-up period. The insets shows that these thermodynamic averages yield better results than the full averages. For the remainder of this project, thermodynamic averages are calculated in this way.

This type of exercise is also useful for analyzing different update functions. Initially I wrote my Monte Carlo program with a simple update function that proposed one single spin flip per Monte Carlo step. This seemed to work, but took a long time to converge ($\approx 10^5$ warm up steps). During

class one day, it was noted that a *Monte Carlo step* should consist of many ($\mathcal{O}(N)$) single spin flip proposals, so that our measurements are much less auto-correlated. This leads to faster convergence with respect to Monte Carlo step, but each Monte Carlo step becomes $\mathcal{O}(N)$ times slower, so in terms of total run-time, this method is much slower. As a result, I also implemented a Wolff cluster update which uses a clever protocol to probabilisticaly construct and then flip a cluster of spins at each Monte Carlo step [2]. This cluster update does scale with system size, whereas the original single spin flip update function does not, but with this update function one needs significantly fewer warm up steps and Monte Carlo steps to obtain good thermodynamic estimates. Thus, the overall computation time needed for Monte Carlo simulations using a cluster update is much lower.

The figures below show E (not a thermodynamic average) as a function of Monte Carlo step for $\beta = 1, 3$ and for each of the three update functions mentioned above. These figures demonstrate how the cluster update function leads to faster convergence. Cluster updates are used in the remainder of this project. Details on how to extend the Wolff cluster update to systems beyond the Ising model can be found in [2] (relevant for the second part of this project).

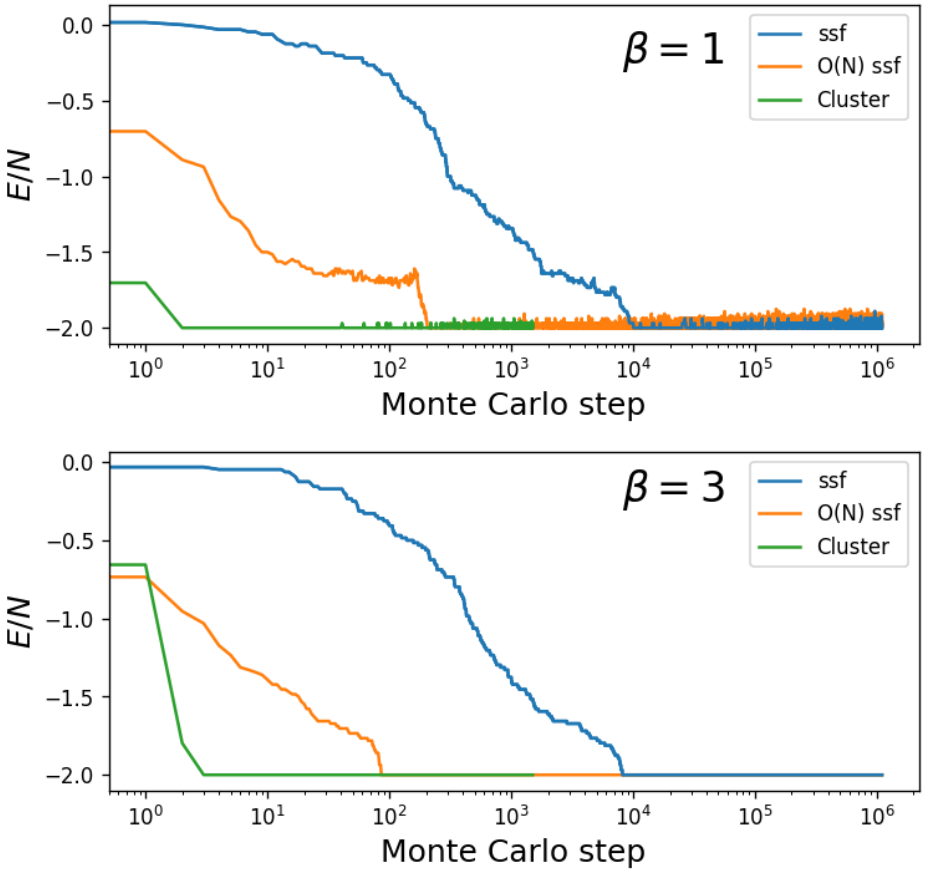

Figure 2: Energy tracked during Monte Carlo simulations using various update functions.

Before proceeding, it is also worth pointing out the different behavior for the different values of β, which is the inverse temperature ($1/T$). As mentioned, each of the described Monte Carlo update

functions accepts a proposed update based on a probability proportional to $\exp(-\beta\Delta E)$, where ΔE is the difference in energy between the original configuration and the proposed update to that configuration. If beta is large and ΔE is positive, then the value of this exponential is very small (and gets smaller with increasing β). This results in proposed configurations rarely being accepted *unless* ΔE is negative (which is favorable when targeting a ground state, and always accepted). The point in bringing this up is to point out that this can be observed in the plots above. For $\beta = 1$, there is still some fluctuation after the warm up period. This is because the value of this exponential value is not too small, so even if a proposed configuration results in a positive ΔE, there is some probability that it will be accepted. On the other hand, for $\beta = 3$, there is very little fluctuation after the warm up period (or after the chain has converged) because β is larger and the probability of accepting a proposed configuration with a higher energy is small.

Part B

Here we examine the thermodynamic averages of the energy and the magnetization, $\langle E \rangle$ and $\langle |M| \rangle$ respectively, as a function of temperature, T.

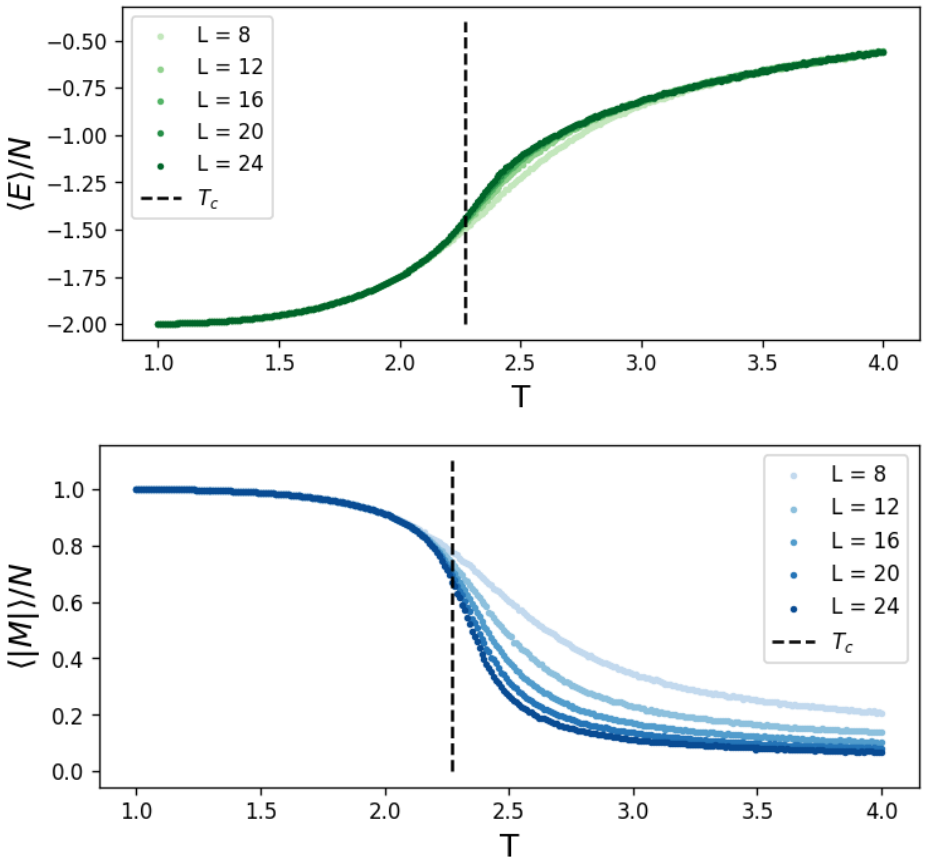

Figure 3: Thermodynamic averages of the energy and magnetization as a function of temperature.

Each data point in the figures above is actually an average over the final values of $\langle E \rangle$ and $\langle |M| \rangle$ for 10 Monte Carlo runs (which I refer to as chains). Because each chain is initialized with a different seed for the random number generator, their behavior over the Monte Carlo steps will differ, but all of the chains should ultimately converge. Averaging over multiple chains keeps one imperfect Monte Carlo run from having a noticeable effect on our analyses. To reiterate what was discussed in Part A, the final values of $\langle E \rangle$ and $\langle |M| \rangle$ for each chain are thermodynamic averages that are estimated over 5000 Monte Carlo steps, each of which involves a Wolff cluster update, and after a warm-up period of 1000 Monte Carlo steps.

In order to see if our simulations agree with theory, I have plotted the magnetization per spin M/N as a function of temperature, T. Note that this is not the absolute value of M/N. Furthermore, I have plotted these values for all 10 chains (for $L = 24$), rather than averaging over the chains.

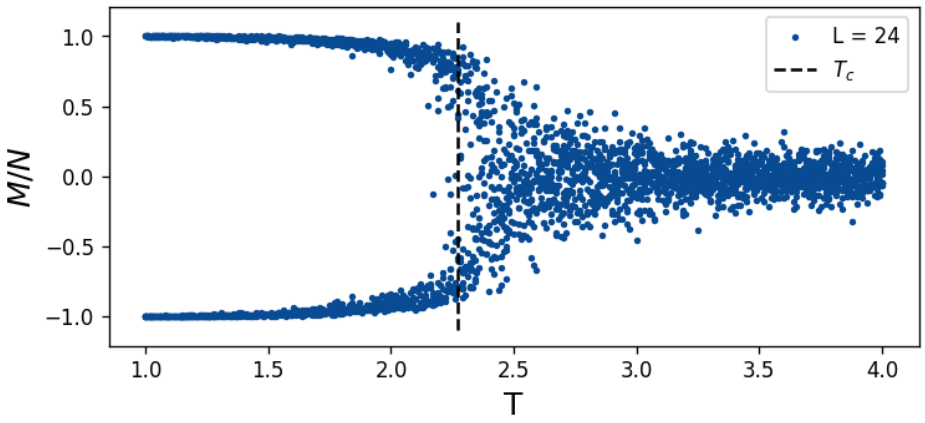

Figure 4: Raw magnetizations as a function of temperature.

According to theory (mean-field theory), as $T \to 0$, there should be two non-trivial values of M that minimize the Free Energy of the system. These two values of M correspond to the two "instances" of the ordered (ferromagnetic) phase, which I discussed above. This behavior is very clearly evidenced in the plot. Plotting the negative and positive results of M/N from all chains, is the only way to visualize that our simulations capture both solutions. In the low temperature regime, the results of my simulations very clean due to the fact that low temperature corresponds to a larger value of β, where, as we saw in Part A, the Markov chain does not "explore" the configuration space much and instead remains firmly in the ground state configuration. On the other hand, theory predicts that as $T \to \infty$, the magnetization, M, should be zero. This is because at high temperature, our model is in the paramagnetic phase, which is a disordered phase where roughly half the spins are spin up and half the spins are spin down. The figure above does agree with this prediction, although there is fluctuation above or below zero. This fluctuation is because high temperature corresponds to smaller values of β, where the Markov chain does explore configuration space more.

Interestingly, this plot is a great visualization of the spontaneous symmetry breaking that occurs during this phase transition. When moving from high- to low-temperature, the system must assume one of the two configurations that minimize the free energy which corresponds to either positive M or negative M, but not both.

Part C

Now that I have established that my simulations give results that are consistent with theory, I can calculate quantities that will allow me to examine the universal behavior of this phase transition. First, using our estimated thermodynamic averages of the energy and the energy squared, $\langle E \rangle$ and $\langle E^2 \rangle$ respectively, I can calculate the specific heat according to the following equation,

$$C_v = \frac{1}{T^2} \left[\langle E^2 \rangle - \langle E \rangle^2 \right]. \tag{4}$$

A derivation for this form of C_v (starting from the definition, $C_v = \partial \langle E \rangle / \partial T$) can be found at the end of this section.

The figures below shows the specific heat, C_v, as a function of temperature, T for various system sizes. The first shows the estimates obtained from averaging our same 10 chains and the second shows an interpolation of these points using a second order polynomial interpolation.

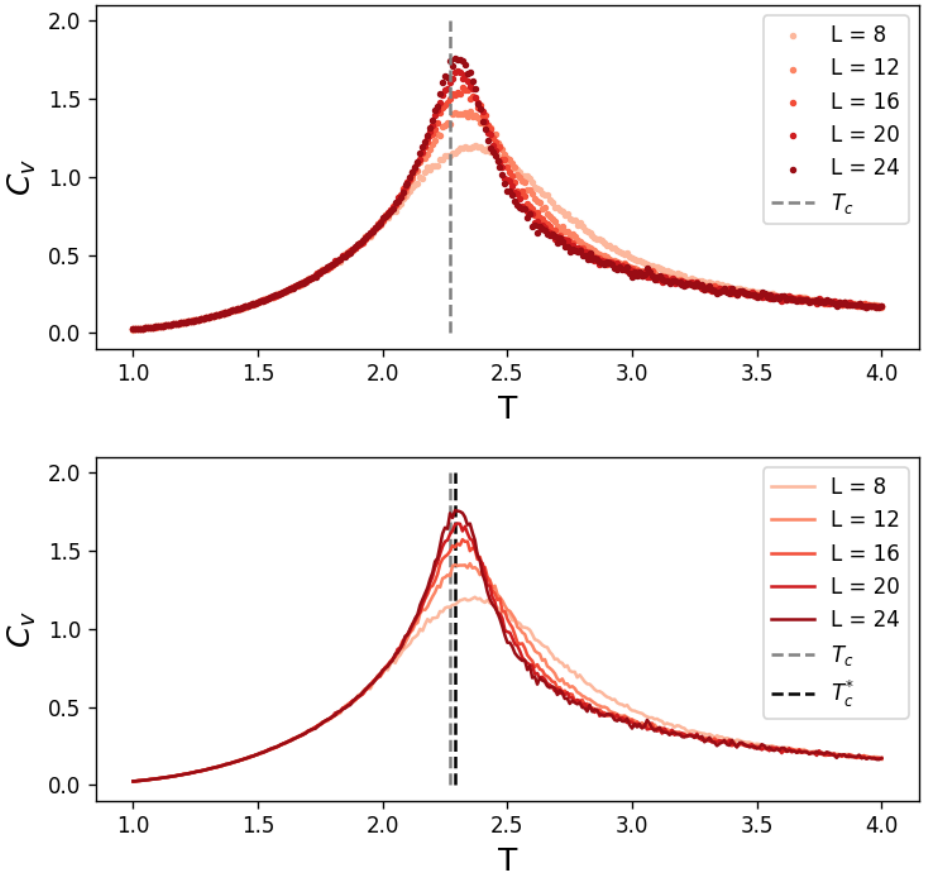

Figure 5: The specific heat as a function of temperature (calculated values and interpolations).

Using the interpolations, I was able to extract the maximum of each curve and estimate the critical temperature for each system size. On the plots above, the exact critical temperature, T_c, is indicated

by the vertical grey line, and the estimate of the critical temperature, T_c^*, is given by the estimate obtained from the largest system size (in this case, $L = 24$) is indicated by the vertical black line. These estimates obtained for other system sizes are summarized in the table below.

	$L = 8$	$L = 12$	$L = 16$	$L = 20$	$L = 24$	Exact
T_c^*	2.37	2.35	2.32	2.30	2.29	$\frac{2}{\log(1+\sqrt{2})} \approx 2.269$

There is a distinct difference between the true critical temperature and the estimate obtained from my simulations. The main reason for this gap is that we are examining finite-size systems of only up to $L = 24$, whereas the exact critical temperature is obtained from calculations carried out in the thermodynamic limit, $N \to \infty$. While there are certainly errors that stem from how I extract these estimates of the critical temperature, it is clear from the curves in the plots above and the trend in my values of T_c^* for each L, that the large part of this discrepancy is due to finite-size effects. Already, as the system size increases, the value of T_c^* improves. The best way to continue systematically improving these results would be to implement even more clever update algorithms that would allow me to look at even larger system sizes. Another technique that often leads to more accurate simulations at and below the critical temperature is the use of annealing. This is a simple method for initializing a Monte Carlo chain at a given temperature, T^*, with the final configuration from the simulation run at a temperature slightly higher than T^*. The other mentioned sources of error include the interpolation method used and the sample error in our thermodynamic averages.

Derivation

First, I will start with the definition of the specific heat,

$$C_v = \frac{\partial \langle E \rangle}{\partial T}, \tag{5}$$

where,

$$\langle E \rangle = \frac{1}{\mathcal{Z}} \sum_{\boldsymbol{\sigma}} E(\boldsymbol{\sigma}) \exp^{(-E(\boldsymbol{\sigma})/T)}, \tag{6}$$

and,

$$\mathcal{Z} = \sum_{\boldsymbol{\sigma}} \exp^{(-E(\boldsymbol{\sigma})/T)}. \tag{7}$$

The following equations are results that will be used in our derivation. First is the temperature derivative of the exponential term that appears in our expectation values and partition function,

$$\frac{d}{dT} \exp^{(-E(\boldsymbol{\sigma})/T)} = \frac{E(\boldsymbol{\sigma})}{T^2} \exp^{(-E(\boldsymbol{\sigma})/T)}. \tag{8}$$

The other is the derivative of our normalization, $1/\mathcal{Z}$,

$$\frac{d}{dT} \frac{1}{\mathcal{Z}} = -\frac{1}{\mathcal{Z}^2} \frac{d\mathcal{Z}}{dT}. \tag{9}$$

Using these definitions and results, I can derive the equation for C_v as a function of $\langle E \rangle$, $\langle E^2 \rangle$, T.

$$\frac{\partial \langle E \rangle}{\partial T} = \left(\frac{d}{dT} \frac{1}{\mathcal{Z}} \right) \sum_{\boldsymbol{\sigma}} E(\boldsymbol{\sigma}) \exp^{(-E(\boldsymbol{\sigma})/T)} + \frac{1}{\mathcal{Z}} \left(\frac{d}{dT} \sum_{\boldsymbol{\sigma}} E(\boldsymbol{\sigma}) \exp^{(-E(\boldsymbol{\sigma})/T)} \right) \tag{10}$$

$$= \left(-\frac{1}{\mathcal{Z}^2} \frac{d\mathcal{Z}}{dT} \right) \sum_{\boldsymbol{\sigma}} E(\boldsymbol{\sigma}) \exp^{(-E(\boldsymbol{\sigma})/T)} + \frac{1}{\mathcal{Z}} \sum_{\boldsymbol{\sigma}} E(\boldsymbol{\sigma}) \frac{E(\boldsymbol{\sigma})}{T^2} \exp^{(-E(\boldsymbol{\sigma})/T)} \tag{11}$$

$$= \left(-\frac{1}{\mathcal{Z}^2} \sum_{\boldsymbol{\sigma}} \frac{E(\boldsymbol{\sigma})}{T^2} \exp^{(-E(\boldsymbol{\sigma})/T)} \right) \sum_{\boldsymbol{\sigma}} E(\boldsymbol{\sigma}) \exp^{(-E(\boldsymbol{\sigma})/T)} + \frac{1}{\mathcal{Z}} \sum_{\boldsymbol{\sigma}} E(\boldsymbol{\sigma}) \frac{E(\boldsymbol{\sigma})}{T^2} \exp^{(-E(\boldsymbol{\sigma})/T)} \tag{12}$$

$$= \frac{1}{T^2} \left[\frac{1}{\mathcal{Z}} \sum_{\boldsymbol{\sigma}} E(\boldsymbol{\sigma})^2 \exp^{(-E(\boldsymbol{\sigma})/T)} - \left(\frac{1}{\mathcal{Z}} \sum_{\boldsymbol{\sigma}} E(\boldsymbol{\sigma}) \exp^{(-E(\boldsymbol{\sigma})/T)} \right)^2 \right] \tag{13}$$

$$= \frac{1}{T^2} \left[\langle E^2 \rangle - \langle E \rangle^2 \right] \blacksquare \tag{14}$$

Part D

Next, I look at the magnetic susceptibility, which can be calculated using the thermodynamic averages of $\langle|M|\rangle$ and $\langle M^2\rangle$ according to the following equation,

$$\chi_T = \frac{1}{NT}\left[\langle M^2\rangle - \langle|M|\rangle^2\right]. \tag{15}$$

A derivation for this form of χ_T (starting from the definition, $\chi_T = (1/N) \times (\partial\langle M\rangle/\partial h)|_{h=0}$) can be found at the end of this section. It is important to note the absolute value taken in the second term in brackets. As seen in Part B, the magnetization can take two values below the critical temperature: one positive and one negative. Therefore, when using the thermodynamic average of the magnetization for this calculation (or any time averaging is done over different chains which may have converged to either of the two solutions), one must consider the thermodynamic average of the absolute value of the magnetization.

The figure below shows the magnetic susceptibility, χ_T, as a function of temperature, T for various system sizes, again taking averages over our same 10 chains.

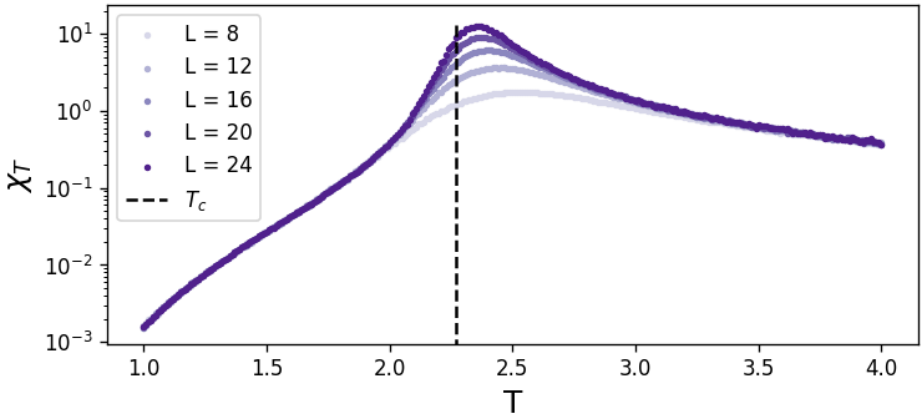

Figure 6: The magnetic susceptibility as a function of temperature.

The curves in this plot can be collapsed by plotting $\chi L^{-\gamma/\nu}$ versus $tL^{-1/\nu}$ [3], where L is the length of the lattice, t is the reduced temperature, $(T - T_c)/T_c$, and γ and ν are the critical exponents, which are the same for any transition in this universality class. Here, I will assume the value of T_c, using the exact value known from theory, and extract estimates for these critical exponents. The figures below show the above curves, collapsed using $T_c = 2/\log(1+\sqrt{2})$ and first, the known values of γ and ν ($\gamma = 7/4$, $\nu = 1$), then second, the values of γ and ν that provide the best collapse ($\gamma = 1.708$, $\nu = 0.949$).

In principle, this collapse should be the best, meaning all of the curves have the best agreement, around T_c, which is $t = 0$. Based on this, I obtained the above estimates for γ and ν by zooming in

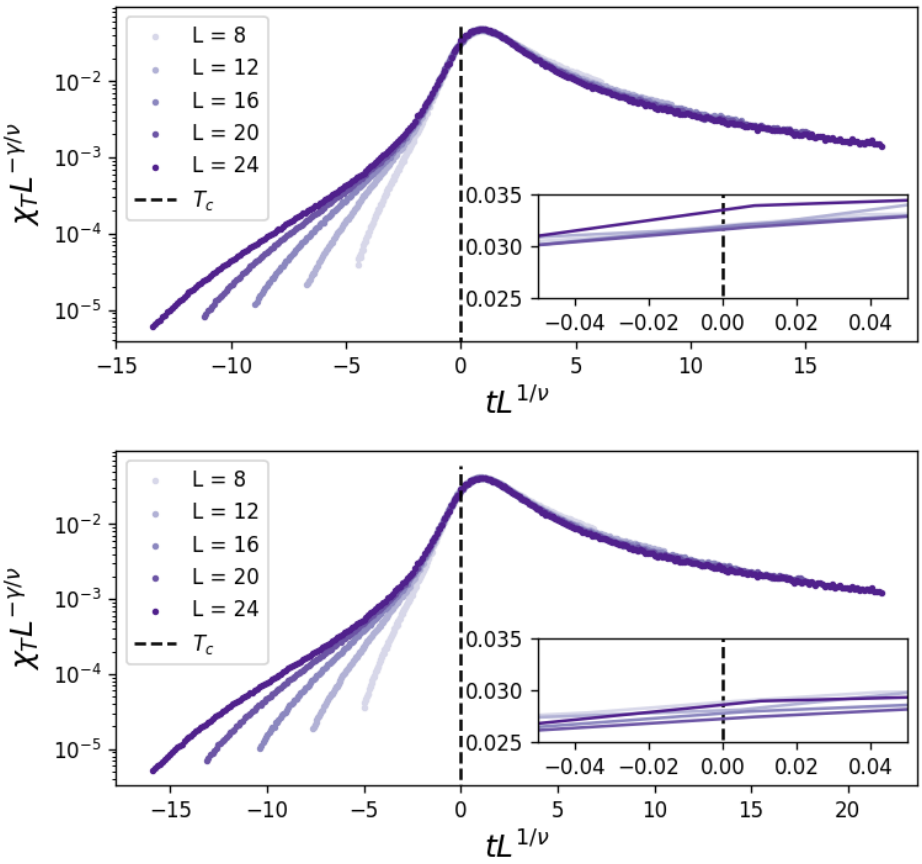

Figure 7: Collapsing χ_T curves with the theoretical values of γ and ν (top) and estimated values of γ and ν (bottom).

to the region around $t = 0$ and adjusting these values until I saw the best agreement. The insets of the above figures show that the estimated values of γ and ν ($\gamma = 1.708$, $\nu = 0.949$) yield slightly better agreement between all the curves. The approach taken here is not a sophisticated approach and, in practice, much more sophisticated methods exist for finding values for critical exponents that yield the best collapse. For example, on could consider the region around $t = 0$, fit a line through the data in that region, and then minimize the variance between the lines corresponding to different system sizes at the point $t = 0$. However, implementing such a method is beyond the scope of this project.

While these estimated values are very close to the theoretical values, it is worth mentioning one of the main sources of error. In addition to other sources of error which have already been mentioned (like sample error in our thermodynamic averages), here, errors in these values arise due to the fact that I assume the critical temperature is that which is given by theory. However, I demonstrated in Part C, that the estimate for the critical temperature given by my simulations, T_c^*, differs from the exact value. Therefore, it does make sense that my curves do not collapse with the theoretical critical exponents for this theoretical value of the critical temperature.

Derivation

First, I will start with the definition of the magnetic susceptibility,

$$\chi_T = \frac{1}{N}\frac{\partial\langle M\rangle}{\partial h}\bigg|_{h=0}, \tag{16}$$

where,

$$\begin{aligned}\langle M\rangle &= \frac{1}{\mathcal{Z}}\sum_{\boldsymbol{\sigma}} M(\boldsymbol{\sigma})\exp^{(-E(\boldsymbol{\sigma})/T)} \\ &= \frac{1}{\mathcal{Z}}\sum_{\boldsymbol{\sigma}} M(\boldsymbol{\sigma})\exp^{(-(E_0(\boldsymbol{\sigma})-hM(\boldsymbol{\sigma}))/T)},\end{aligned} \tag{17}$$

and,

$$\mathcal{Z} = \sum_{\boldsymbol{\sigma}} \exp^{(-(E_0(\boldsymbol{\sigma})-hM(\boldsymbol{\sigma}))/T)}. \tag{18}$$

Here, it is important to note that our energy function has a term linear in the magnetization, M, that is proportional to h, the reduced magnetic field. In the end, we take $h \to 0$, but this term is needed in order to take the derivative with respect to h.

The following equations are results that will be used in our derivation. First is the derivative of the exponential term that appears in our expectation values and partition function with respect to h,

$$\frac{d}{dh}\exp^{(-(E_0(\boldsymbol{\sigma})-hM(\boldsymbol{\sigma}))/T)} = \frac{M(\boldsymbol{\sigma})}{T}\exp^{(-(E_0(\boldsymbol{\sigma})-hM(\boldsymbol{\sigma}))/T)}. \tag{19}$$

The other is the derivative of our normalization, $1/\mathcal{Z}$,

$$\frac{d}{dh}\frac{1}{\mathcal{Z}}\bigg|_{h=0} = -\frac{1}{\mathcal{Z}^2}\frac{d\mathcal{Z}}{dh}\bigg|_{h=0}. \tag{20}$$

Using these definitions and results, I can derive the equation for $\partial\langle M\rangle/\partial h$ as a function of $\langle|M|\rangle$, $\langle M^2\rangle$, and T.

$$\frac{\partial\langle M\rangle}{\partial h} = \left(\frac{d}{dh}\frac{1}{\mathcal{Z}}\right)\sum_{\boldsymbol{\sigma}} M(\boldsymbol{\sigma})\exp^{(-(E_0(\boldsymbol{\sigma})-hM(\boldsymbol{\sigma}))/T)} + \frac{1}{\mathcal{Z}}\left(\frac{d}{dh}\sum_{\boldsymbol{\sigma}} M(\boldsymbol{\sigma})\exp^{(-(E_0(\boldsymbol{\sigma})-hM(\boldsymbol{\sigma}))/T)}\right) \tag{21}$$

$$= \left(-\frac{1}{\mathcal{Z}^2}\frac{d\mathcal{Z}}{dh}\right)\sum_{\boldsymbol{\sigma}} M(\boldsymbol{\sigma})\exp^{(-(E_0(\boldsymbol{\sigma})-hM(\boldsymbol{\sigma}))/T)} + \frac{1}{\mathcal{Z}}\sum_{\boldsymbol{\sigma}} M(\boldsymbol{\sigma})\frac{M(\boldsymbol{\sigma})}{T}\exp^{(-(E_0(\boldsymbol{\sigma})-hM(\boldsymbol{\sigma}))/T)} \tag{22}$$

$$= \left(-\frac{1}{\mathcal{Z}^2}\sum_{\boldsymbol{\sigma}}\frac{M(\boldsymbol{\sigma})}{T}\exp^{(-(E_0(\boldsymbol{\sigma})-hM(\boldsymbol{\sigma}))/T)}\right)\sum_{\boldsymbol{\sigma}} M(\boldsymbol{\sigma})\exp^{(-(E_0(\boldsymbol{\sigma})-hM(\boldsymbol{\sigma}))/T)} + \frac{1}{\mathcal{Z}}\sum_{\boldsymbol{\sigma}} M(\boldsymbol{\sigma})\frac{M(\boldsymbol{\sigma})}{T}\exp^{(-(E_0(\boldsymbol{\sigma})-hM(\boldsymbol{\sigma}))/T)} \tag{23}$$

$$= \frac{1}{T}\left[\frac{1}{\mathcal{Z}}\sum_{\boldsymbol{\sigma}} M(\boldsymbol{\sigma})^2\exp^{(-(E_0(\boldsymbol{\sigma})-hM(\boldsymbol{\sigma}))/T)} - \left(\frac{1}{\mathcal{Z}}\sum_{\boldsymbol{\sigma}} M(\boldsymbol{\sigma})\exp^{(-(E_0(\boldsymbol{\sigma})-hM(\boldsymbol{\sigma}))/T)}\right)^2\right] \tag{24}$$

Therefore, taking $h \to 0$, I can conclude,

$$\chi_T = \frac{1}{N}\frac{\partial\langle M\rangle}{\partial h}\bigg|_{h=0} \tag{25}$$

$$= \frac{1}{TN}\left[\langle M^2\rangle|_{h=0} - (\langle M\rangle^2)|_{h=0}\right] \blacksquare \tag{26}$$

Problem 4: Two-Dimensional XY Model

Using all of the tools developed for the Ising model, we can replace our Ising spins with two-dimensional "rotors" which are defined by continuous variables, $0 < \theta_i < 2\pi$, and study the two-dimensional XY model. This model is defined by the following Hamiltonian,

$$\hat{H} = -\sum_{\langle ij \rangle} \cos(\theta_i - \theta_j), \tag{27}$$

where θ_i, θ_j are the angles that define these rotors, and we still consider nearest neighbor interactions, $\langle ij \rangle$. I again consider finite-size square lattices with periodic boundary conditions. I study system sizes up to $L = 24$.

This model has continuous symmetries, in contrast to the Ising model which has discrete Z_2 symmetry. According to the Mermin-Wagner theorem, this means there is no long-range order and thus, no spontaneous symmetry breaking in one- and two-dimensional systems [4]. As a consequence, there is no conventional phase transition associated with sponatneous symmetry breaking, as was the case for the Ising model. However, a finite-temperature phase transition does exist for this system (Kosterlitz-Thouless), at a temperature T_{KT}. Analytically solving a related, but approximate, model gives an estimate for the critical temperature, $T_{KT} \approx 0.8816$ [5] and state of the art Monte Carlo simulations give $T_{KT} \approx 0.8935(1)$ [6].

In order to obtain an estimate of T_{KT} from my finite-size Monte Carlo simulations, I track the thermodynamic averages of the energy, energy squared, and the spin stiffness, ρ_s, which is defined in a particular lattice direction, a, by the following equation,

$$\rho_s = \frac{1}{N} \left\langle \sum_{\langle ij \rangle_a} \cos(\theta_i - \theta_j) \right\rangle - \frac{1}{TN} \left\langle \left[\sum_{\langle ij \rangle_a} \sin(\theta_i - \theta_j) \right]^2 \right\rangle. \tag{28}$$

The first thing we are asked to do for this model is to plot the "acceptance rate" of our Monte Carlo simulations as a function of temperature, T. This is the rate at which a proposed update is accepted. This is, of course, dependent on the update function used. At first, I implemented the suggested Monte Carlo update, which is one in which the proposed configuration is obtained by rotating each rotor by a (different) random angle. It is important to point out that this is a global update, in that each of the rotors is changed in the proposed configuration. This is not always desirable (as I will show). It is also worth noting that, since this is a continuous model, the updates become more computationally expensive, as the changes in energy are no longer discrete (and thus, they cannot be stored and quickly recalled). This made these simulations extremely slow, as evidenced by the smaller system sizes. The figure below shows the acceptance rates (from using the described update function) as a function of temperature T, for multiple system sizes.

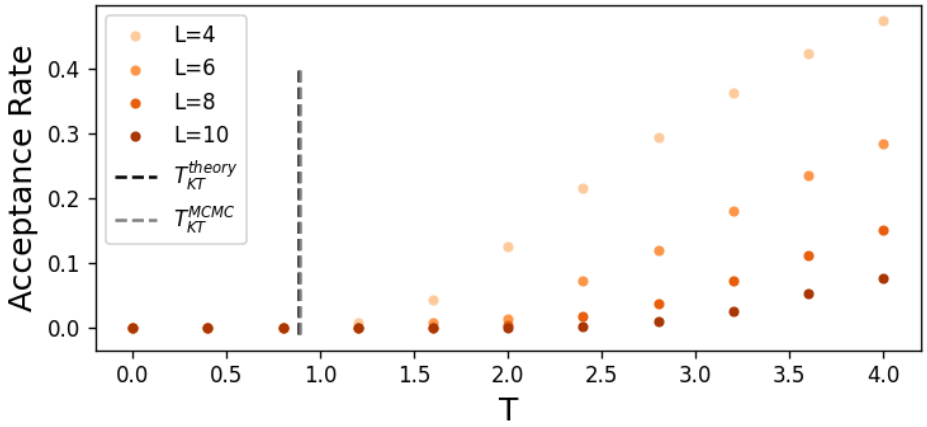

Figure 8: Acceptance rates as a function of temperature.

The acceptance rates decay quickly to zero with decreasing temperature. This makes sense, since we only accept a proposed update when the value of $\exp(-\beta\Delta E)$ is larger than some random number. As T gets very small, β gets very large and the value of $\exp(-\beta\Delta E)$ also gets very small unless ΔE is considerably large. But, as discussed, this global update involves adjusting *every* rotor, and the odds of favorably adjusting enough of these rotors to have a considerably large ΔE, is very small. With any update function that relies on the value of $\exp(-\beta\Delta E)$, the acceptance rate will go down as T gets smaller (β gets larger). This was also demonstrated in Part A for the Ising model when I compared the behavior of Monte Carlo energies for $\beta = 1, 3$. Here, the acceptance rates for low T are so small, that it is likely that our Markov chains are unable to converge to accurate energies (at least in a reasonable amount of time). Furthermore, I have shown on the plot the theorized and numerically obtained values for T_{KT} to show that this behavior in the acceptance rate occurs well before the phase transition (i.e. for $T > T_{KT}$). This means that with this update function, I had little hope of observing anything interesting.

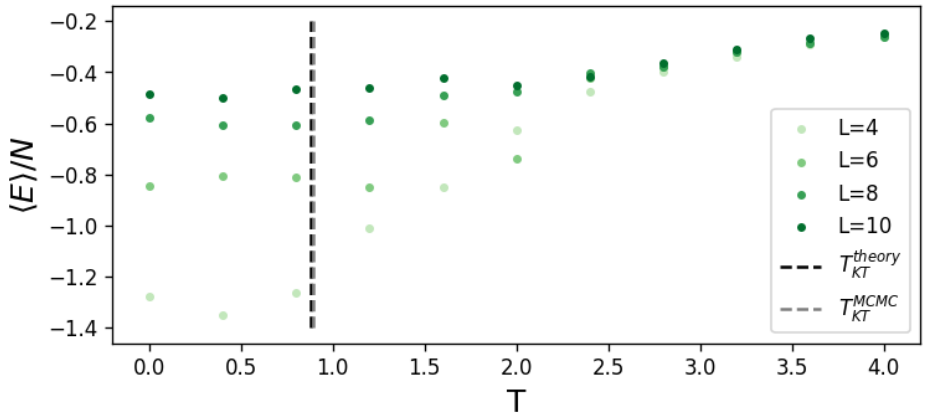

Figure 9: Thermodynamic averages of the energy as a function of temperature.

To confirm my hypothesis about non-converging Markov chains due to extremely small acceptance rates, I plotted the thermodynamic average of the energy per spin, $\langle E \rangle / N$, as a function of temperature, T, for the system sizes I simulated (Fig. 9). The behavior clearly confirms my hypothesis, with the low-temperature simulations performing worse as system size, L, increases. The system size dependence comes from the fact that this is a global update, and a favorable proposal gets less likely the more rotors there are in the system being adjusted at each step. This is also consistent with the fact that for larger systems, the acceptance rate becomes small at higher temperatures. Based on these observations, I implemented a cluster update, which is a generalization of the Wolff cluster update that I implemented for the Ising model [2].

Using this cluster update, I only needed 1000 warm up steps and 5000 Monte Carlo steps to obtain accurate thermodynamic averages of the energy for system sizes up to $L = 24$. It's worth pointing out that this is much larger than the system sizes that were accessible to me when using the global update discussed above. This is because I needed orders of magnitude fewer Monte Carlo steps. The results of these simulations are shown in the figure below.

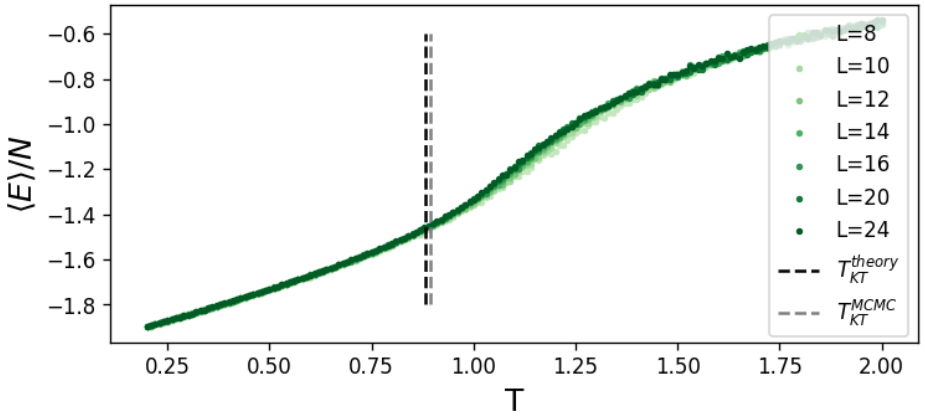

Figure 10: Thermodynamic averages of the energy as a function of temperature. Obtained with Monte Carlo simulations using a cluster update function.

Using these energies, I was also able to calculate the specific heat as a function of temperature, T, which is shown in Fig. 11 below. In the previous part of this project (Part C), we extracted the critical temperature, T_c, from the peak of the specific heat curves. In these figures, I have included the theoretical and numerically-predicted values for T_{KT} to show that this approach does not work here. The peaks in the specific heat curves are, in this case, misleading, and do not correspond to the temperature at which the phase transition occurs. Instead, the phase transition can be detected by measuring the spin stiffness in a lattice. One can measure this spin stiffness in arbitrary lattice direction (i.e. for $a = x, y$ for 2D systems) using Eqn. (28). Figure 12 below shows spin stiffness (averaged over both the x and y directions) as a function of temperature, T.

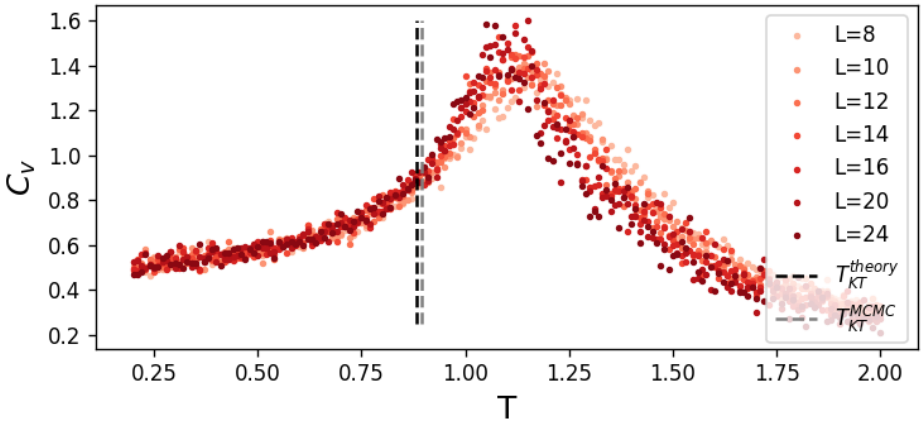

Figure 11: The specific heat as a function of temperature.

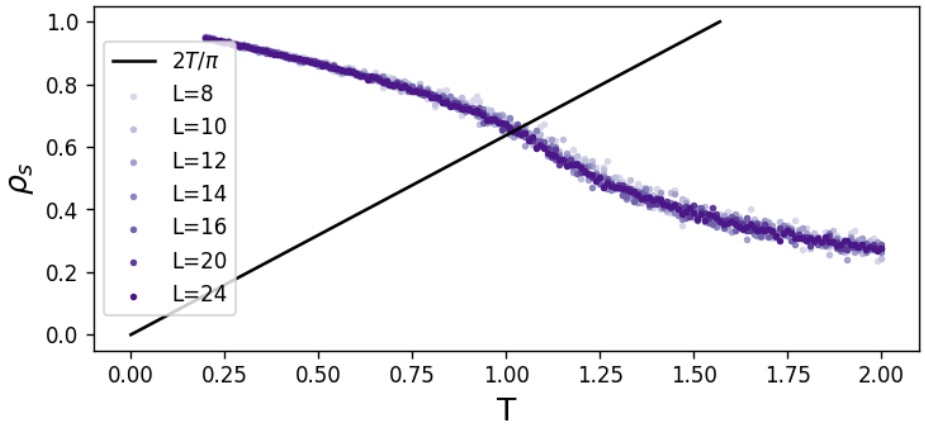

Figure 12: Spatially averaged spin stiffness as a function of temperature.

The universal relationship between the spin stiffness and the critical temperature is summeraized by the following equation,

$$\rho_s(T_{KT}) = \frac{2T_{KT}}{\pi}. \tag{29}$$

Therefore, in order to estimate T_{KT} from the above spin stiffness results, I plotted $2T/\pi$ as a function of T and obtained an estimate for the critical temperature, T^*_{KT}, for each system size by finding the point at which the $\rho_s(T)$ curve intersects with the line $2T/\pi$. In order to do this, I fit a line to the points in the region very near to this intersection. Obviously $\rho_s(T)$ does not linearly depend on the temperature, which is why I consider only a small region near the intersection. These linear fits are shown in Fig. 13 below. Using the results of these linear fits, I was able to extract the estimates of the critical temperature for each system size. These estimates are summarized in the table below.

	$L=8$	$L=10$	$L=12$	$L=14$	$L=16$	$L=20$	$L=24$
T^*_{KT}	1.04	1.03	1.025	1.03	1.027	1.022	1.022

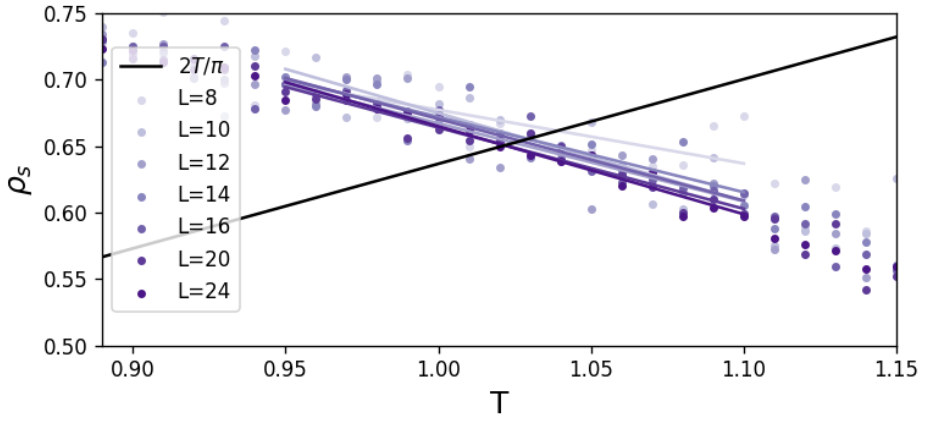

Figure 13: Linear fits to the spin stiffness near the intersection with $2T/\pi$.

Recalling from class that the correlation length scales as, $\xi \propto \exp(-\text{const.}/\sqrt{T - T_{KT}})$, we can use finite size scaling to derive the following equation relating $T^*_{KT}(L)$ to T_{KT},

$$T^*_{KT}(L) = T_{KT} + \frac{\text{const.}^2}{\ln^2(L)}. \tag{30}$$

Therefore, by plotting our values for $T^*_{KT}(L)$ versus $1/\ln^2(L)$, we can fit a line through our data points and extract the y-intercept as an approximation for T_{KT}. Note that the y-intercept is the value of the above equation when $L \to \infty$, which corresponds with the thermodynamic limit. The figure below shows this finite-size scaling using the results from my Monte Carlo simulations.

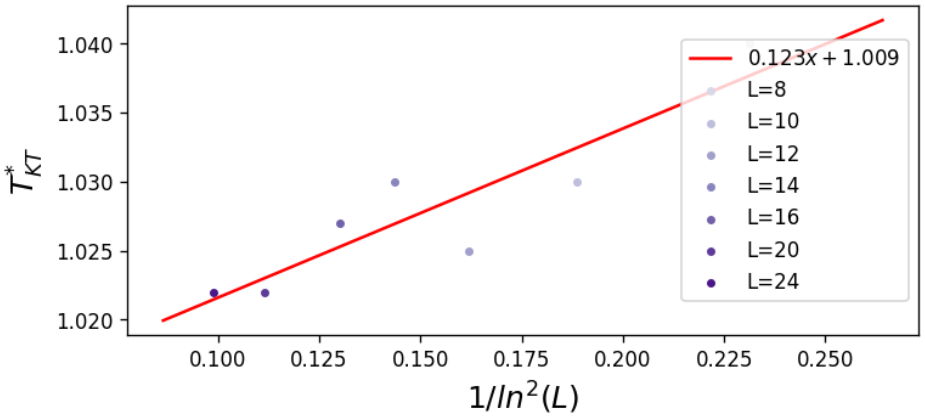

Figure 14: Finite-size scaling to obtain the critical temperature, T_{KT}.

The red line is the fit to my linearized data, and the parameters of this fit are shown in the legend. Based on this fit, I estimate $T_{KT} = 1.009$. While this is significantly higher than both the theoretical and the numerical estimates for T_{KT}, it is at least the same order of magnitude.

Similar to what was seen in the first part of this project (Part D), it is clear that as the systems get larger, the value of T_{KT} gets smaller and slightly closer to the true value. This indicates that the

finite size of my simulations do have an effect on the estimated values of the critical temperature. However, the improvement in T^*_{KT} with system size is not significant enough to write off all error as finite-size effects. Taking one step back, there is a clear trend in the spin stiffness as a function of temperature, however, for all examined system sizes, there is considerable fluctuation. This has a large effect on the values of T^*_{KT} since we are using a linear fit through a region of this data. One way to at least minimize these fluctuations would be to average over more than 10 chains. Perhaps then, there would be a clearer trend in spin stiffness as a function of lattice size, L, which is not clear from my simulations (as seen in the plots and the table above). As a result, the line fit through my linearized data (Fig.14) had a coefficient of determination (R^2), a value that tells me how well the statistical model fits the data, of only 0.82. Hence, if the trend in ρ_s, and thus, T^*_{KT}, with respect to L were stronger, this fit would hopefully be better in two ways: providing a better fit to $T^*_{KT}(L)$ and also yielding a more accurate estimate of T_{KT}.

References

[1] L. Onsager, "Crystal statistics. i. a two-dimensional model with an order-disorder transition," *Phys. Rev.*, vol. 65, pp. 117–149, Feb 1944.

[2] U. Wolff, "Collective monte carlo updating for spin systems," *Physical Review Letters*, vol. 62, no. 4, p. 361, 1989.

[3] A. W. Sandvik, "Computational studies of quantum spin systems," in *AIP Conference Proceedings*, vol. 1297, pp. 135–338, American Institute of Physics, 2010.

[4] N. D. Mermin and H. Wagner, "Absence of ferromagnetism or antiferromagnetism in one- or two-dimensional isotropic heisenberg models," *Phys. Rev. Lett.*, vol. 17, pp. 1133–1136, Nov 1966.

[5] D. C. Mattis, "Transfer matrix in plane-rotator model," *Physics Letters A*, vol. 104, no. 6, pp. 357–360, 1984.

[6] Y.-D. Hsieh, Y.-J. Kao, and A. W. Sandvik, "Finite-size scaling method for the berezinskii–kosterlitz–thouless transition," *Journal of Statistical Mechanics: Theory and Experiment*, vol. 2013, no. 09, p. P09001, 2013.